Surlyn®/Silicate Hybrid Materials. I. Polymer *In Situ* Sol–Gel Process and Structure Characterization

DAVID A. SIUZDAK,* PAUL R. START, KENNETH A. MAURITZ

Department of Polymer Science, University of Southern Mississippi, Hattiesburg, Mississippi 39406-0076

Received 11 June 1999; accepted 11 November 1999

ABSTRACT: We report the creation of a new organic/inorganic hybrid material that results from sol–gel reactions for tetraethylorthosilicate (TEOS) within poly[ethylene-*co*-methacrylic acid], as well as within a Zn^{+2} partially neutralized form of this copolymer (Surlyn®). FTIR and ^{29}Si solid-state NMR spectroscopic probes yield information regarding molecular connectivity within the *in situ* grown silicate structures. FTIR analyses of Surlyn® matrix bands suggest that strong molecular level interactions between the organic and inorganic phases are not present, although there is other evidence that these phases are mechanically coupled on a larger dimensional scale. The ^{29}Si solid-state NMR analyses indicate mainly Q_3 and Q_4 coordination states about the SiO_4 substructures, regardless of silicate content, which is in general agreement with the interpretation of the FTIR results that show incomplete condensation. Environmental scanning electron microscopy and energy dispersive X-ray analysis results reinforce the conclusion that a significant silicate component is incorporated deep within TEOS-treated films. Differential scanning calorimetry studies of Surlyn®-Zn^{+2}/silicate hybrids suggest that silicate incorporation essentially does not disrupt crystallinity. Thermogravimetric analyses show practically no change in the degradation onset temperature, which is consistent with organic/inorganic phase separation. The general conclusion is that a silicate phase can indeed be incorporated within this acid copolymer, as well as its Zn^{+2} ionomeric form, via *in situ* sol–gel processes. © 2000 John Wiley & Sons, Inc. J Appl Polym Sci 77: 2832–2844, 2000

Key words: Surlyn®; silicate; sol–gel process; nanocomposite; characterization

INTRODUCTION

Surlyn®, a random, semicrystalline copolymer of ethylene (E) and methacrylic acid (MAA), typically is within the range of 2–7 mol % MAA composition and is commercially available in the acid, or partially neutralized ($X^+ = Na^+$ or Zn^{+2}) forms:

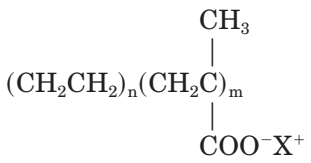

While the quantity of literature regarding the structure, properties, and processing of this commercial polymer is great, we only call attention to prior studies that are relevant to the experimental results reported here. Wilson et al.[1,2] discovered a small angle X-ray scattering (SAXS) peak for the ionomer form that persisted well above the melting temperature (T_m) up to 300°C. This feature was taken to be the signature of ionic clusters that have sizes of around a few nanometers, as crudely depicted in Figure 1. Counterion-ex-

Correspondence to: K. A. Mauritz (kenneth.mauritz@usm.edu).

**Present address:* Lilly Industries, Inc., 521 W. McCarty Street, Indianapolis, IN 46225.

Contract grant sponsors: Mississippi NSF-EPSCoR program; E. I. DuPont de Nemours & Co.

Journal of Applied Polymer Science, Vol. 77, 2832–2844 (2000)

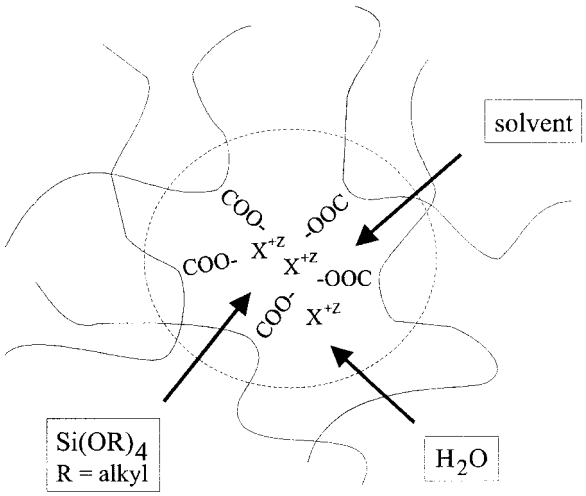

Figure 1 An ionic cluster on the order of a few nanometers in size. These clusters are considered preferred sites in the ionomeric form for inorganic oxide nanoparticle formation via *in situ* sol–gel reactions for tetraethoxysilane. The solvent is also expected to reside outside the clusters.

changed Surlyn® possesses mechanical properties superior to those of polyethylene (PE) for a given molecular weight (MW) that is due to these clusters. Improved tensile strength, toughness, grease resistance, and puncture and abrasion resistance and good gas barrier properties, optical clarity, and heat sealability led to important commercial applications of this thermoplastic ionomer.[3–5]

On first heating in a differential scanning calorimeter, E-MAA copolymers and their ionic forms exhibit two endotherms at approximately 60 and 90°C as reported by Tadano et al.[6] The high temperature transition corresponds to the PE crystallite melting at T_m. In the process of cooling from above T_m, only one peak, due to PE recrystallization, appears at ~44°C. Upon second heating, but *soon* after first cooling, only the transition at T_m is present and the low temperature transition is absent. However, when the same samples are stored at room temperature after the first cooling, the low temperature peak reappears upon reheating and becomes stronger while shifting to higher temperatures with increased storage time. The "domains" whose disordered structures are frozen-in during cooling from above the T_m become ordered again upon annealing.

There are conflicting views about the structure in which this lower temperature transition takes place. Tadano et al. assigned this history-dependent endotherm to an order–disorder transition in ionic clusters at a temperature they termed T_i, and the reader is referred to their publications in which this theory was rationalized and supportive evidence presented.[6–8] More recent IR spectroscopic studies of E-MAA ionomers by these investigators are also interpreted in a way that supports their ionic aggregate transition model.[9] It should be pointed out that their view does not appear to be in harmony with the later appearing model of Eisenberg et al. that redefines clusters to include contiguous regions of restricted chain mobility about smaller ionic multiplets.[10] In the revised view of Eisenberg et al. the idea of an ionic domain glass transition was replaced by a concept of the onset of chain segmental mobility in these restricted mobility regions.[10] Also, the DSC and wide and small angle X-ray scattering (WAXS/SAXS) investigations of E-MAA ionomers by Cooper et al. suggested that the low temperature endothermic event is due to the melting of thin lamellar crystallites.[11,12] These secondary crystallites are said to be prevented from thickening because carboxylic acid and salt groups act as defects that cannot be incorporated into thick crystal lamellae. Secondary crystallization is thought to develop over time as a gradual reordering occurs through annealing within amorphous domains. Recently, the time-resolved SAXS/WAXS studies of Loo and Register demonstrated the existence of secondary crystals that form between the primary lamellae on slow cooling or aging and that these secondary crystals melt in the same range where the low temperature differential scanning calorimetry (DSC) endotherm occurs.[13] These investigators also call attention to a similar secondary crystal formation that takes place in nonionic ethylene copolymers [e.g., poly(ethylene terephthalate)[14]] and mention that this low temperature endotherm is, in fact, not unique to ionomers. The Cooper et al.[11,12] and Tadano et al.[6–8] groups both show DSC peaks at a "T_i" for *unneutralized* E-MAA in which there are no ionic aggregates, which directly indicates that ionic domains are not implicated in the lower temperature transition. Our own DSC studies for acid form Surlyn® are in harmony with these results. Otocka et al.[15] found that the DSC thermograms of annealed but unquenched *unneutralized* ethylene acrylic acid copolymers show basically the same double endotherms as the similar E-MAA and their ionomeric forms. Clearly, the results of Otocka et al. cannot implicate ionic domains in their similar semicrystalline copolymers that contain no ionic aggregates.

In another realm of material science, Mauritz et al.[16–30] created a number of organic–inorganic hybrids via polymer *in situ* sol–gel reactions for inorganic alkoxides, alkyl-alkoxysilanes, and mixtures thereof. These materials included poly(*n*-butyl methacrylate)/TiO_2,[16] poly(ether sulfone)/SiO_2,[17,18] Nafion®/SiO_2,[19–21] Nafion®/[SiO_2-TiO_2],[22,23] Nafion®/[SiO_2-Al_2O_3],[19] Nafion®/ZrO_2,[24] Nafion®/[organically modified silicate],[25–27] an alkoxide-functionalized Nafion® SO_2F precursor,[28] [perfluoro-carboxylate/sulfonate (bilayer)]/SiO_2,[29] and poly(styrene-*b*-isobutylene-*b*-styrene)/SiO_2 hybrids.[30]

In this article we report on *in situ* sol–gel reaction schemes aimed at creating novel Surlyn®/silicate hybrids. In particular, we discuss direct and indirect probes of the structures of the incorporated silicate phases and the polymer matrix using FTIR and ^{29}Si solid-state NMR spectroscopies, environmental scanning electron microscopy/energy dispersive analysis using X-rays (ESEM/EDAX), DSC, and thermogravimetric analysis (TGA). We regard these semicrystalline ionomers as matrices that influence the *in situ* polymerization of inorganic alkoxide monomers and the structure of the resultant dry inorganic oxide phase. It is our working hypothesis that a limited sol → gel process initiates within the ionic clusters of ionized Surlyn® or perhaps at the sites of —COOH groups in the un-ionized acid form polymer, given the presence of water, according to the usual hydrolysis and polyfunctional condensation reactions:

$$\equiv SiOR + H_2O \rightarrow \equiv SiOH + ROH;\ 2(\equiv SiOH) \rightarrow \equiv Si-O-Si\equiv + H_2O, \text{ etc.}$$

The monomer used in these studies was tetraethylorthosilicate (TEOS).

Our initial transmission electron microscopic (TEM) studies indeed revealed the presence of nonagglomerated, rather spherical silicate particles that were dispersed throughout the Surlyn® matrix upon sample drying.[31] Owing to the fact that these particles have diameters on the order of 10s of nanometers and a relatively narrow size distribution, these hybrid materials qualify as "nanocomposites." Because nanoparticles can be grown in both the acid and ionomeric forms, it was concluded that the presence of ionic aggregates is not a necessary condition for nanocomposite formation. Because phase separation exists on a scale sufficiently smaller than the wavelengths of light, no appreciable scattering occurs within films of these materials, which is a desirable property with regard to the use of these materials in the form of packaging films.

In earlier work we studied the influence of sol–gel-derived silicate phases on selected properties of Surlyn®.[32] For example, the tensile modulus increases while elongation at break decreases with increasing silicate uptake. The melt flow index of the filled H form is lower than that of the unfilled H form but it is higher than that of the partially Zn^{+2} neutralized unfilled form. FTIR analysis of hybrids previously subjected to the melt flow experiment showed that the silicate phase remained intact but that the high temperatures in this device drove condensation reactions between SiOH groups. In another experiment, after *in situ* sol–gel reactions and drying, [Surlyn®-H]/silicate flakes were passed through an extruder to assess the effect of melt processing conditions on the silicate structure. All silicate IR fingerprint bands for the processed hybrid persisted and the spectrum closely resembled that of a nonextruded hybrid, including the signature of the Si—OH groups. ^{29}Si solid-state NMR spectroscopy was used to probe the degree of molecular connectivity within the silicate phase. The spectrum was consistent with those of nonextruded hybrids in that Si atom coordination around SiO_4 units was predominantly Q_3 and Q_4, the bias in the distribution toward Q_3 being in harmony with the IR results.

EXPERIMENTAL

Film Preparation

In an effort to identify an optimal method for producing quality Surlyn® films for inorganic modification, two methods were evaluated: solution casting and melt pressing. In solution casting the binary solvent xylene/*n*-butanol was chosen. Whereas xylene dissolves the PE phase, the polar end group on *n*-butanol molecules disrupts structures around ionic domains. An 85:15 (v/v) mixture provided rapid, complete dissolution. Base resin (H^+ form, 5.8 mol % MAA) and partially neutralized (23% Zn^{+2} counterion exchanged, 5.8 mol % MAA) forms were both examined. The partially neutralized form was considerably more difficult to dissolve, presumably because of divalent Zn^{+2} counterions acting as ionic crosslinks between —COO^- groups. Films were obtained by this method, but the reproducibility and quality of the films were marginal.

Melt pressing yielded reproducible, void free films. A Carver model C lab press was used, along with poly(tetrafluoroethylene) coated steel substrates to facilitate ease of sample removal. All films were processed at 115°C for 5 min, then immediately quenched using an aluminum heat sink; the temperature dropped to ~30°C within 30 s. The sole procedural exception was the application of a melt temperature of 180°C for a specific set of Zn^{+2} neutralized Surlyn® films for FTIR spectroscopic analysis, which was due to more difficult processing rheology.

Film Swelling and *In Situ* Sol–Gel Reactions

Experiments were performed to identify a solvent that maximizes film swelling to enhance the permeation and *in situ* sol–gel reactions of TEOS molecules. A homologous series of aliphatic alcohols, as well as two polar aprotic solvents (THF, DMAc), were chosen for these studies. Equilibrium swelling in the alcohols showed a clear trend of increasing solvent uptake with increasing alkyl length, which is reasonable considering the long PE blocks within Surlyn®. DMAc and THF were too robust and damaged the film integrity within hours; 1-propanol was selected as the solvent of choice. Higher alcohols displayed apparent miscibility problems in the presence of the quantity of H_2O used for TEOS hydrolysis.

In situ sol–gel reactions were preceded by swelling melt pressed films (1–5 mil thick) for 24 h in 1-propanol, followed by the addition of a 4:1 (mol/mol) H_2O:TEOS aliquot. This H_2O:TEOS ratio corresponds to complete TEOS hydrolysis, although this condition may not be realized in practice. Acid or base catalyst was neither added nor needed in these experiments, which proceeded for prescribed times to achieve a variety of inorganic uptakes. After given TEOS permeation–reaction times, the samples were removed from the solution bath and flushed with 1-propanol to remove possible silica precipitates on the film surfaces. Then the samples were placed in a vacuum oven at 50°C and 1 Torr for a minimum of 24 h. This step removes volatiles from the film and further drives the condensation reactions between SiOH groups within the silicate phase. Also, the release of solvent might influence the ease with which chains can pack into secondary crystallites. After this drying–annealing step, all the samples were simultaneously placed in a dessicator for a few days before each of the experiments was performed. Thus, all of the samples used for a given characterization experiment experienced the same thermal-aging history.

Silicate mass (m) uptake is expressed as $(m_{\text{final}} - m_{\text{initial}})/m_{\text{initial}} \times 100\%$. Uptakes as high as 104% were achieved and the films remained optically transparent, although a whitelike tint was observed at higher loadings. The composite films remained flexible with no signs of cracking with uptakes as high as 90%.

FTIR Spectral Analysis

This technique was used to verify the incorporation of a silicate phase to the extent that Si—O—Si bonds were formed. Qualitative conclusions regarding the degree of intramolecular connectivity of this phase can be made by observing the signature of uncondensed SiOH groups. Spectra were obtained using a Bruker 88 spectrophotometer with the resolution fixed at 4 cm^{-1}. The thickness of the films under test were on the order of 1 mil.

^{29}Si Solid-State NMR Analysis

The ^{29}Si solid-state NMR experiments were conducted to study the degree of molecular connectivity of the silicate phase. We discussed peak assignments for different degrees of Si atom substitution about the SiO_4 tetrahedra in earlier reports of organic/silicate hybrids.[14,15,19,20,23–25] Peaks are denoted by the symbol Q^n for the Si atom coordination state $(RO)_{4-n}\mathbf{Si}(OSi)_n$, where R = H or an alkyl group. Each peak is located within a range of chemical shifts relative to $Si(Me)_4$ as follows: $Q^1 = -68$ to -83 ppm, $Q^2 = -74$ to -93 ppm, $Q^3 = -91$ to -101 ppm, and $Q^4 = -106$ to -120 ppm.

Solid-state NMR spectra were acquired using a Bruker MSL-400 NMR spectrometer operating at a frequency of 79.5 MHz for ^{29}Si. A standard double air bearing cross polarization/magic angle spinning probe was used. Samples were loaded into 4-mm fused zirconia rotors and sealed with Kel-F™ caps. Spectra were obtained using magic angle spinning with high power decoupling during acquisition only and a spinning rate of ~4500 Hz. A modified version of the DEPTH sequence[33] was used to suppress ^{29}Si background due to the probe. The 90° pulse width was ~4 μs, the probe dead time was 13 μs, and the acquisition time was 45 ms. The recycle delay was 180 s. All chemical shifts were referenced externally to the downfield peak of tetrakis(trimethylsilyl)silane (-9.8 with respect to TMS).

ESEM/EDAX

The ESEM/EDAX experiments were conducted as in our earlier studies to confirm the presence of an

in situ grown silicate phase from a different perspective. EDAX analysis was used to determine silicon elemental and therefore silicate compound concentration profiles across composite film thicknesses. Only Zn^{+2} exchanged Surlyn® was examined in these intitial studies because Zn is of sufficiently detectable atomic weight to serve as an internal composition reference for the polymer. The X-ray intensity of a particular elemental line at its characteristic energy was divided by that observed for Zn to yield the relative concentration of the former. The film was freeze fractured in liquid N_2 and X-ray analysis was conducted on a cross section.

DSC Analysis

DSC was used to determine whether the incorporated silicate phases influence the Surlyn® thermal transitions discussed earlier. This analysis was performed using a Mettler DSC 30/S ThermoAnalytical device; the temperature program consisted of ramping from −100 to 170°C at a rate of 10°C/min, followed by a −50°C/min quench to −100°C. This process destroys the thermal history of the sample. Following quenching, samples were reheated according to the same temperature program and thermograms were obtained.

TGA

TGA was used to characterize unfilled control and silicate-filled Surlyn®-H films to assess whether organic–inorganic phase interactions influence thermal degradation. Samples were placed in alumina crucibles and tested using a Mettler Toledo TGA850 instrument with a thermal ramp over the range of 25–550°C at the rate of 20°C/min.

RESULTS

FTIR Spectroscopy

IR spectral studies of unfilled E-MAA copolymers and their ionomers were reported by Earnest and MacKnight[34] and Brozoski et al.[35] The former were mainly concerned with hydrogen bond formation between carboxylic acid dimers while the latter analyzed coordination structures of carboxylate groups about different cations within ionic multiplets. The primary and limited goal of the IR studies presented in this article was to isolate characteristic bands of the silicate phase by subtracting, from the spectrum of a given Surlyn®/silicate film, the spectrum of the unfilled Surlyn®

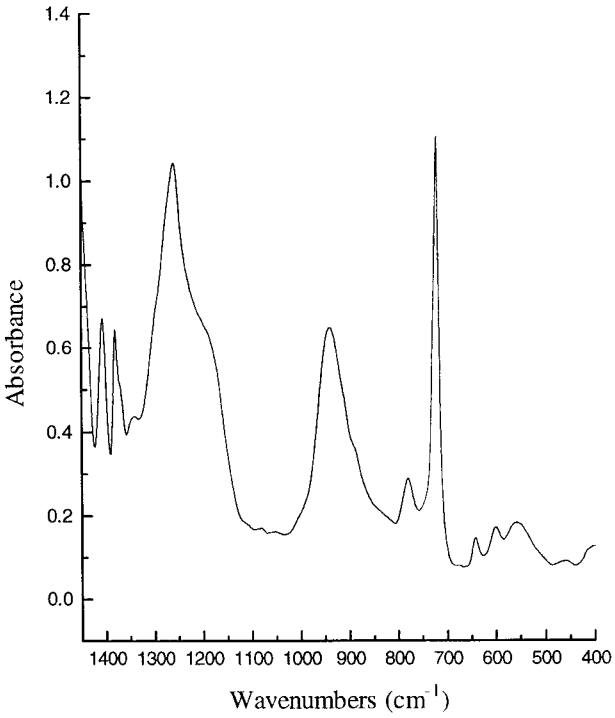

Figure 2 An FTIR transmission spectrum of unmodified Surlyn®–H.

film that has identical copolymer composition, cation type, and degree of neutralization for an ionomer form. Brief comments are offered in regard to bands for the Surlyn®-H matrix, although a more detailed IR analysis, with a view toward organic–inorganic phase interactions, will be conducted in the future. Subtraction of the transmission spectrum of an untreated Surlyn®-H film from the spectrum of the same, but TEOS-modified, film uncovers bands that are clear fingerprints of a silicate phase. The pure Surlyn® spectrum in Figure 2 is truncated above ~1450 cm^{-1} because of the strong absorption at higher wave numbers, regardless of film thickness, as well as the fact that this region is beyond that in which the silicate bands of interest reside. The sharp band at ~720 cm^{-1} seen in Figure 2 is due to methylene rocking in the backbone of Surlyn®.[36] While this is not a silicate, but is instead a polymer band, attention is called to it here because the difference spectra of TEOS-modified films reveal a vestige of this peak that is due to incomplete subtraction, perhaps because of minor changes in the percentage of crystallinity (PE crystal field splitting[37]) in the Surlyn® template.[38] While this band appears as a singlet in Figure 2, a closer inspection reveals twin peaks, as discussed later in this report. Carboxylic acid

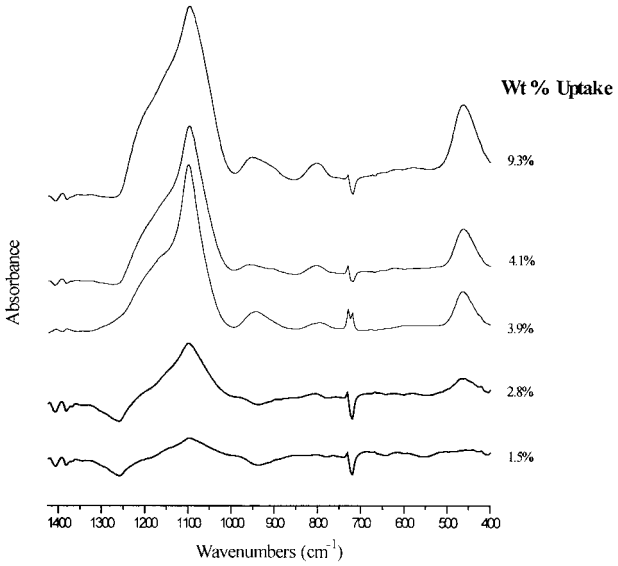

Figure 3 FTIR difference spectra of Surlyn®–H/silicate hybrids with the indicated inorganic weight percent uptakes.

dimerization is mainly studied using the band at ~1700 cm^{-1}, although Van Alsten showed that the analysis of this peak is complicated by ion neutralization that affects a shift to lower wave numbers.[39] COOH dimerization is also characterized by a broad out of plane O—H bending peak at ~940 cm^{-1} that is also seen in Figure 2.

Figure 3 consists of the difference spectra of Surlyn®-H having the indicated percent silicate uptakes. The broad band centered at ~1100 cm^{-1} for Surlyn®-H that has silicate uptakes from 1.5 to 9.3% is attributed, as in our previous studies of Nafion®/silicate nanocomposites,[19,25] to the asymmetric stretching vibration of Si—O—Si groups because it is in the correct region for this mode, it becomes more distinct with increasing silicate content, and it does not exist in the spectrum of unfilled Surlyn®-H in this region. This band is important because it provides evidence of successful condensation reactions between Si—OR and/or Si—OH groups.

A distinct shoulder at ~1200 cm^{-1} on the left side of this asymmetric Si—O—Si band is present on all the spectra in Figure 3 and is in the region of C—O—C stretching for ester groups.[40] It might seem reasonable to assume that the reaction COOH + PrOH → COOPr + H_2O occurred to some extent during the preliminary leaching step because the solvent used was 1-PrOH. Added to this, the shoulder at 1200 cm^{-1} is present in the spectrum for unfilled Surlyn®-H in Figure 2 and there is no silicate peak that could in this region. However, as will be seen later, the intrinsically strong C═O asymmetric stretching band for COOPr, which should occur in the 1720–1750 cm^{-1} region, is not present and this fact eliminates the possibility of ester formation, at least at the IR-detectable level. This peak corresponds to the polymer matrix rather than to the silicate phase, but the fact that it is also observed on difference spectra suggests that it may have been shifted as the result of the polymer *in situ* sol–gel reactions. Kutsumizu et al. mention a band at ~1260 cm^{-1}, corresponding to the C—O stretching vibration of COOH groups in hydrogen bonded dimers, as coupled with the O—H in-plane bend, for E-MAA ionomers.[9] This mode, of course, also exists for aliphatic carboxylic acid small molecules. It is conceivable that this mode might be shifted to lower wave numbers by hydrogen bonding interactions between —COOH and ≡SiOH groups so that it is not subtracted from the composite spectrum, although this would be conjecture.

A peak for Si—OR stretching, which reflects unhydrolyzed alkoxide groups, would appear at somewhat less than 1100 cm^{-1} but there is no clear evidence of this fingerprint.

The peak at ~950 cm^{-1}, the so-called network "defect band," is due to Si—OH stretching and it is a clear signature of incomplete condensation reactions.[19,41,42] It is reasoned that this band is not associated with carboxylic acid dimers because it increases in absorbance with increasing silicate content. Of course, it must be allowed that a residue of the dimer band could persist due to imperfect spectral subtraction and the close proximity of these bands could cause a minor distortion of the Si—OH absorbance envelope. In considering that the integrated absorbance of this defect band is significant as compared to that of the asymmetric Si—O—Si band, a substantial degree of incomplete molecular connection must exist in the silicate phase. A peak seen at ~800 cm^{-1} might be due to symmetric stretching in Si—O—Si groups. While this vibration is theoretically IR inactive, its presence, which provides additional evidence of successful condensation reactions, might be due to a deformation of tetrahedral bonding symmetry about Si atoms as discussed in our earlier studies of polymer/silicate hybrids. Finally, the strong and broad band at ~450 cm^{-1} that increases in absorbance with increasing silicate content is assigned, as in earlier studies of Nafion®/silicate nanocomposites, to Si—O—Si bending vibration. The considerable widths of these peaks is attributed to a broad

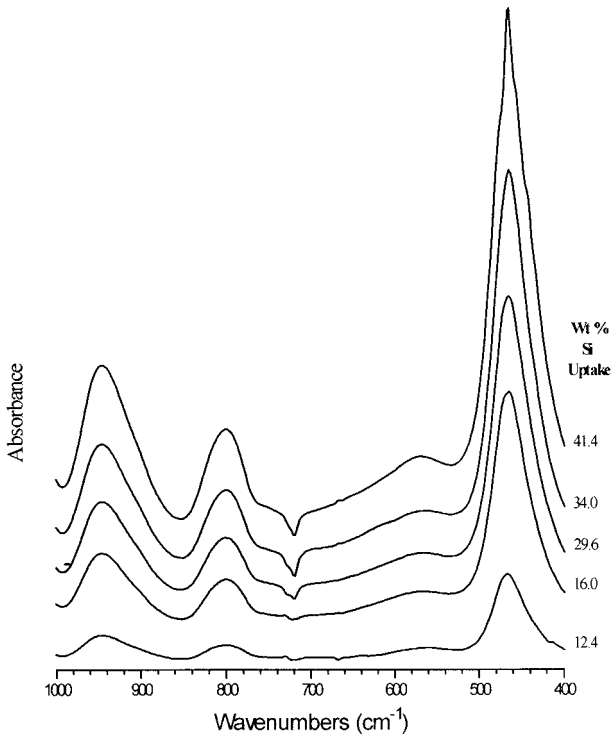

Figure 4 FTIR difference spectra of Surlyn®–Zn^{+2}/silicate hybrids with the indicated inorganic weight percent uptakes.

distribution of the molecular environment about vibrating groups that are bonded in silicate phases that are known to consist of highly dispersed, high surface/volume, amorphous nanoparticles.[31] Thus, all of the fingerprint bands of a silicate phase are present and Figure 3 shows that they become more distinct with increasing silicate content. This behavior is also seen in Figure 4, which contains difference spectra for the Zn^{+2} neutralized composites. These facts led us to believe that the subtraction spectrum is truly representative of the silicate phase as incorporated within the Surlyn® polymeric template but with some interference caused by imperfect spectral subtraction. Moreover, a silicate phase can be incorporated in both the acid and ionomeric forms as shown by IR spectroscopy.

In order to study perturbations of the polymer matrix caused by the embedded silicate component, it is necessary to inspect the composite spectra because the matrix bands cannot be isolated. This poses a limitation on the quality of information that can be obtained because of the overlapping of certain silicate with adjacent polymer bands. Here we offer comments on selected Surlyn®-H bands and reserve a more detailed analysis for a future report.

The 850–1000 cm^{-1} region, which is expanded in Figure 5, contains the clear signature of the out of plane OH bending vibration in COOH dimers for 0% silica.[43] The spectra are vertically displaced for better visualization. It should be pointed out that the 0% spectrum that is subtracted from each composite is taken from a different corresponding sample in each case (i.e., the 0% curve in Fig. 5 is not a universal control). It is noted that the spectrum for Surlyn®-H/(0.39% silica) and its unfilled Surlyn®-H control can be rather well superimposed, which suggests an inability to detect an incorporated silicate structure in this part of the spectrum at this low level. While the peak wave number does not shift when proceeding to higher uptakes, the distribution width increases. Furthermore, the difference spectra in Figure 3 show a distinct band that is always positive in this region. There are two situations that might account for this net absorbance upon subtraction. The first is the silicate component might perturb the hydrogen bonding structure of carboxylic acid dimers, say by interactions with ≡SiOH groups, so as to affect a broader distribution of this vibration frequency. However, this "flattening" of the peak would result in a negative absorbance upon subtraction, given that the total number of —COOH groups (i.e., copolymer composition) is constant, and a negative peak is in fact not observed. The second situation is that because of the fact that the Si—OH stretching vibration occurs exactly in this region, its absorbance envelope simply adds to the band for carboxylic acid dimers. The latter explanation seems to be most reasonable.

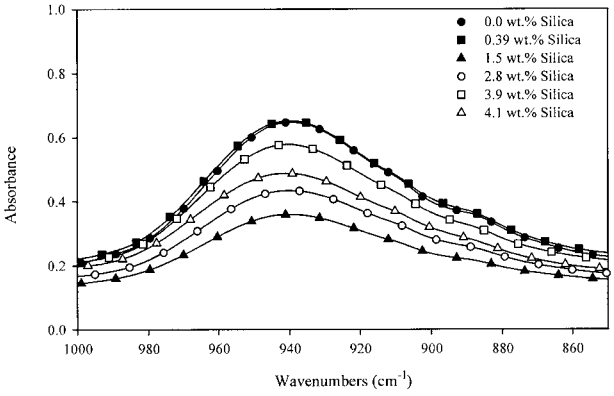

Figure 5 FTIR spectra (unsubtracted) of Surlyn®–H/silicate hybrids and an unfilled Surlyn®–H control in the region of the out of plane OH bending vibration for carboxylic acid dimers. The spectra are vertically displaced for better visualization.

Earnest and MacKnight pointed out that in Surlyn®, the absorbance for the C═O stretching vibration in hydrogen bonded carboxylic acid dimers, where both C═O groups are in hydrogen bonds, occurs at ~1700 cm^{-1} and that this vibration for free carboxylic acid groups (i.e., neither the C═O nor C—O—H group of the same COOH unit is in a hydrogen bond) absorbs at ~1750 cm^{-1}.[34] These authors noted that the free carbonyl band for Surlyn® is very weak and only becomes appreciable at high temperatures. Coleman et al. report that the band for the case in which the C═O group is free, but the OH group is in a hydrogen bond, occurs at a position between these two wave numbers.[44] It should also be mentioned that Earnest and MacKnight stated that a band at 1735 cm^{-1} is due to carbonyl groups from oxidation products.[34] A shoulder (or shoulders) on the main carbonyl peak at ~1700 cm^{-1} does in fact appear in the 1750–1725 cm^{-1} region in the spectra in Figure 6 for both the unfilled control and the composites. The vertical scale is greatly expanded to illustrate this feature. The weakness of this shoulder is in harmony with the conclusion of Earnest and MacKnight[34] that acid dimerization is rather complete at room temperature and it appears that the *in situ* sol–gel process that leads to the incorporation of silicate does not alter this fact.

Also seen in Figure 6 is a somewhat asymmetric band that consists of a peak at ~1470 cm^{-1} and a weak shoulder at ~1440 cm^{-1}. The main peak is in a region of overlap of peaks for methylene scissoring and asymmetric methyl bending

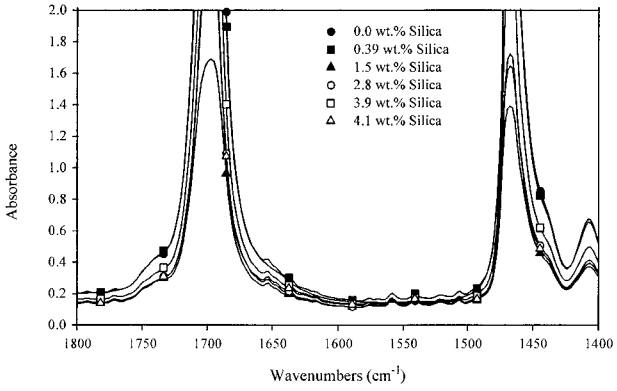

Figure 6 FTIR spectra (unsubtracted) of Surlyn®–H/silicate hybrids and unfilled Surlyn®–H control in the region of carbonyl stretching in free and hydrogen bonded carboxylic acids groups (left) and methylene scissoring and asymmetric methyl bending (right) vibrations. The spectra are vertically displaced for better visualization.

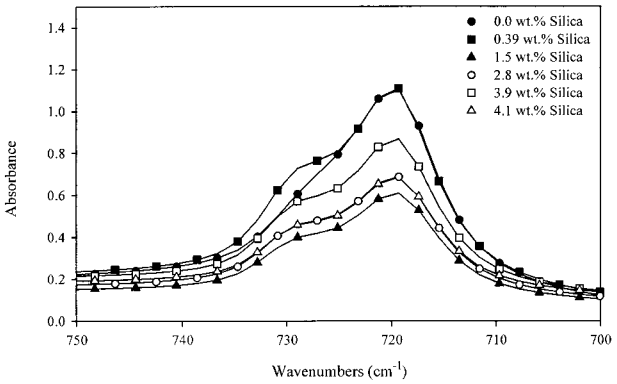

Figure 7 FTIR spectra (unsubtracted) of Surlyn®–H/silicate hybrids and unfilled Surlyn®–H control in the region of the CH_2 rocking vibration.

deformations.[45] Neither of these two absorbances suffers a frequency shift with silicate incorporation.

Consider again the band for CH_2 rocking at ~720 cm^{-1}, which is expanded for closer inspection in Figure 7. This absorbance envelope consists of a single peak for the unfilled Surlyn®-H control, but it acquires a distinct shoulder on the high wave number side (~730 cm^{-1}) when the silicate component is added. This shoulder is not in the vicinity of any band associated with silicate structures. Painter and Coleman[37] discuss the phenomenon of crystal field splitting in PE that is given evidence by the doublets at 733/721 and 1460/1475 cm^{-1}. Perhaps the doublet seen in Figure 7 is due to crystal field splitting because our DSC results show a strong melting endotherm reflective of crystallinity. This assignment suggests that the 1470/1440 cm^{-1} pair seen in Figure 6 is the second doublet associated with crystal field splitting. However, the unfilled control in this particular case does not exhibit the first doublet, although it is observed for other control samples and the 1470/1440 cm^{-1} pair is faintly visible for the unfilled control. Thus, it is inconclusive as to whether crystal field splitting actually exists in the filled polymer. In the difference spectra for the composites, a negative absorbance is usually seen at the low wave number peak position and a positive absorbance at the shoulder position. The negative difference peak can be mathematically accounted for by a decreased intensity of the main peak, and the presence of the positive peak would arise from an increase in intensity of the shoulder relative to the respective intensities of the corresponding unfilled controls.

The overall lack of frequency shifting of the Surlyn®-H associated bands with the incorpora-

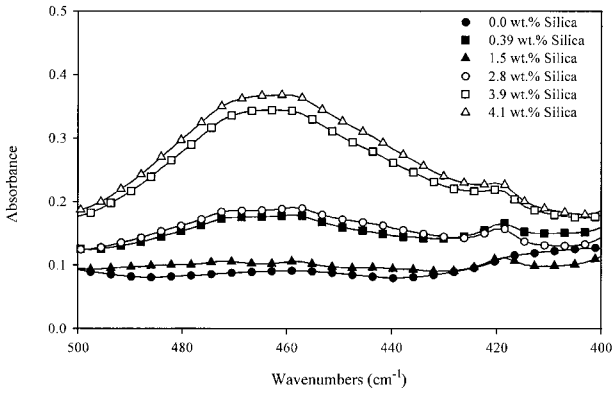

Figure 8 FTIR spectra (unsubtracted) of Surlyn®–H/silicate hybrids and unfilled Surlyn®–H control in the vicinity of the peak for Si—O—Si bending deformation (left).

tion of the silicate component suggests, in general terms, a lack of strong *molecular level* interactions between the organic and inorganic phases to the extent that bond polarization is affected. Of course, this result does not preclude interactions on higher dimensional scales. For example, an entrapment or interlocking of polymer chains within microscopic pockets at the surface of the silicate nanoparticles is possible. While the particles appear spherical under TEM examination,[31] it is possible that their surfaces are "rough" at a higher level of magnification. In any case, interfacial interactions of some sort must be present to account for the observed trend in mechanical tensile properties versus silicate content.[32]

An interesting feature, not seen in Figure 3, emerges when the spectrum in the limited 500–400 cm^{-1} region is expanded. This feature is seen in Figure 8 and consists of a peak at ~420 cm^{-1} to the right of the peak assigned to Si—O—Si bending deformation at ~450 cm^{-1}. This trait appears in the spectra for composites with no peak frequency variation, but it is absent in the spectrum for unfilled Surlyn®. Therefore, it is most likely that this peak is associated with the silicate phase, although we are presently unable to make an assignment in terms of a specific molecular vibration mode.

The spectra for the composites based on Zn^{+2} neutralized Surlyn®, which are shown in Figure 4, are truncated above 1000 cm^{-1} so that the silicate signature bands at lower wave numbers can be seen more distinctly because the Si—O—Si asymmetric stretching peak for samples having ≥16 wt % uptake, which is also present for these modifications, is very strong. The same conclusions offered above for the Surlyn®-H based hybrids are essentially true for the Surlyn®-Zn^{+2} based hybrids: all the silicate signature bands are present and become more pronounced with increasing inorganic content, and there are a number of uncondensed SiOH groups. Again, vestiges of the methylene rocking band remain on these spectra.

In some experiments involving short TEOS permeation times, negative silicate percentage weight uptakes were observed. This suggested that the leaching of Surlyn® oligomers occurred during the solvent swelling step, especially because slightly turbid solutions were seen after swelling. To test for this, films were swollen in 1-PrOH for ≥24 h, removed, and placed *in vacuo* and the remaining 1-PrOH solution was evaporated as well. A gummy, tacky residue remained in the vessel and this was examined via FTIR transmission spectroscopy. A comparison of the residue spectra with that of a nonswollen Surlyn® film supports the concept of the outleaching of a low molecular weight fraction because all of the Surlyn® bands were present in the former, as shown in Figure 9.

Consequently, to minimize this mass loss in the swelling step prior to the *in situ* sol–gel reaction for TEOS, pressed films were first subjected to a leaching step in 1-PrOH for a minimum of 24 h, followed by drying to constant weight *in vacuo*. Subsequent swelling, followed by TEOS permeation and ensuing sol–gel reactions, occurred as described previously. Mass loss was still present, albeit low (<1%, and even less for Zn^{+2} neutralized species).

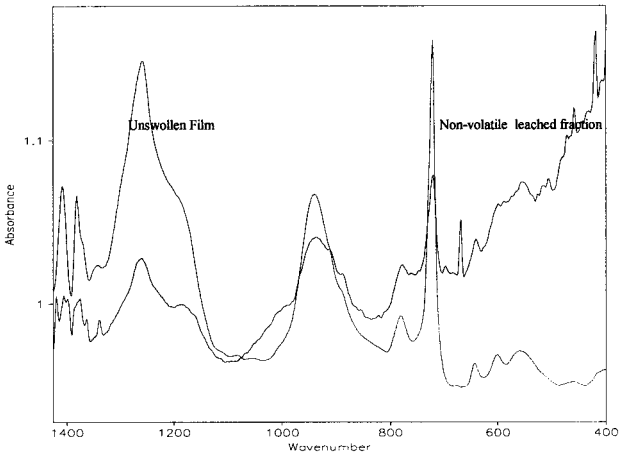

Figure 9 FTIR spectra of (a) unswollen Surlyn® and (b) the nonvolatile residue remaining after evaporation of the swelling solvent.

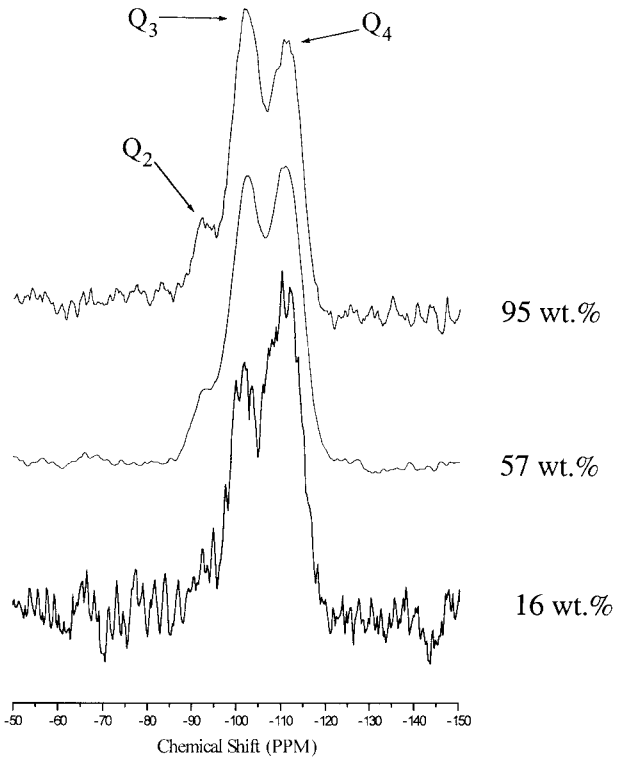

Figure 10 ^{29}Si solid-state NMR spectra of Surlyn®–H hybrids with the indicated silicate weight percentages.

^{29}Si Solid-State NMR Spectroscopy

The spectra for 16, 57, and 95 wt % silicate are displayed in Figure 10. The spectrum of the 95% hybrid, which is mostly silicate, should have a spectrum that does not reflect the confining effects of, and interactions with, the Surlyn®-H matrix. The chemical shift distribution consists almost exclusively of Q_3 and Q_4 species, regardless of silicate content, although some Q_2 character is seen above the noise in the top two spectra. It is reasonable to think that "porous" silicate nanoparticles will have a considerable degree of intramolecular disconnection, although these particular spectra are not of such a quality as to resolve, say, the Q unit sequence distributions that might be correlated with a measured porosity. The considerable degree of Q_3, as well as detectable Q_2, coordination is in general agreement with the structural interpretation of the FTIR results and it might be inferred that some degree of porosity is present. The relative population of SiO_4 groups that are coordinated to four Si atoms is comparable to the fraction that has incomplete coordination.

ESEM/EDAX

A plot of the Si:Zn X-ray intensity ratio across the fracture surface of a film having 7 wt % silicate in Figure 11 shows a relatively constant concentration of Si with somewhat higher concentrations near the film edges. While the points are scattered and the data should be viewed on a semiquantitative basis, the concentration of Si compared to Zn is somewhat high. Perhaps using Surlyn® with a greater degree of neutralization and greater percentage of MAA would minimize this statistical error because Zn is used as the internal X-ray standard or reference against which the Si X-ray absorption is measured. Nonetheless, the evidence in Figure 11 reinforces the conclusion, arrived at by spectroscopic means, that a significant silicate component is successfully incorporated through the depth of the film whose thickness is ~5 mils.

DSC Analysis

Two endothermic transitions are seen on a *first heating* run of an unfilled Surlyn®-H control sample in Figure 12. It is important to note that these transitions are inherent to the acid form, as well as the counterion-exchanged form. The higher temperature (T_m = ~90°C) endotherm is assigned to the melting of primary crystallites, based on knowledge derived from the earlier stud-

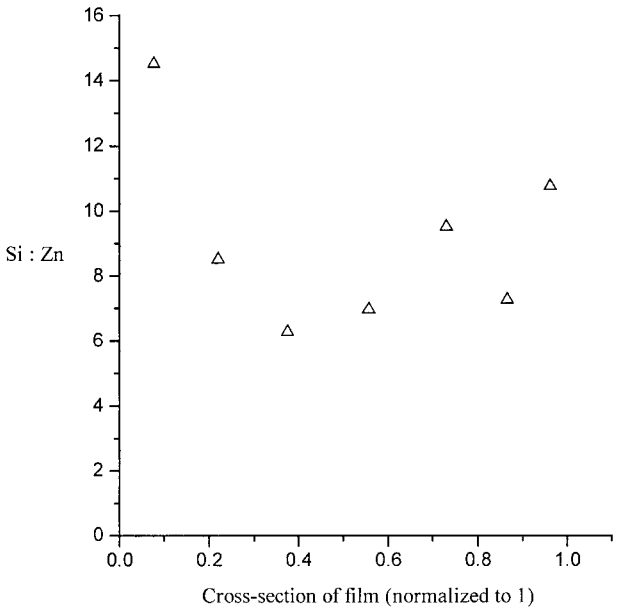

Figure 11 Si:Zn relative concentration profile across the thickness direction of a Surlyn®–Zn^{2+}/silicate film with 7 wt % silicate as determined by ESEM/EDAX.

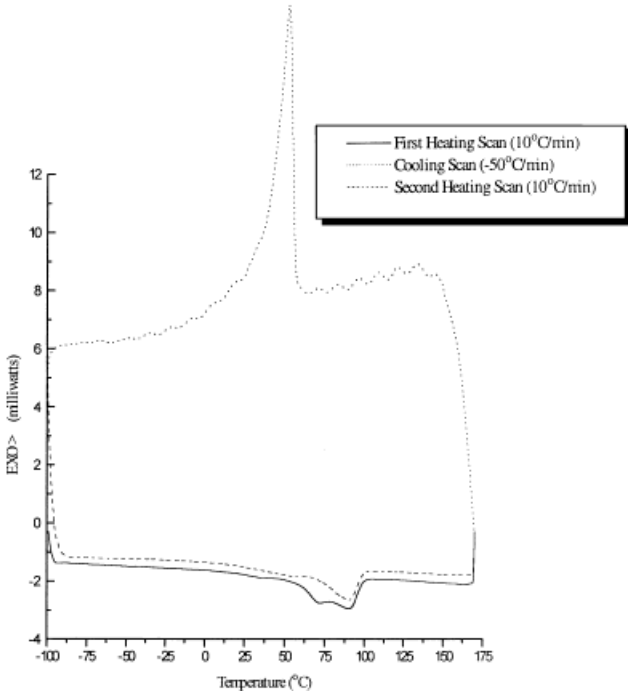

Figure 12 First-heating, cooling, and second-heating DSC scans for unmodified Surlyn®–H.

ies discussed in the Introduction. The lower temperature (which we label as T_m') endotherm occurs between 40 and 70°C. Based on the evidence presented in the Introduction, we tentatively assign this event to the melting of small *secondary* crystallites as possibly modified by the presence of silicate structures. During quenching, a crystallization exotherm is observed at ~50°C. Upon subsequent reheating, the lower endotherm disappears. However, when annealed at ambient temperature for times on the order of days or weeks, this submelting temperature event reappears. The exact position of T_m', as discussed by Kutsumizu et al., is a function of aging time.[8]

Next, we discuss the DSC thermograms of TEOS-modified Surlyn® samples. *First-scan* thermograms for Surlyn®-Zn^{+2}/silicate hybrids are seen in Figure 13 and reveal two distinct endotherms similar to those seen for the unmodified Surlyn® control in Figure 12. T_m' and T_m are relatively unchanged with silicate incorporation. It must be kept in mind that the samples in Figure 13 are not pure Surlyn® but are Surlyn®-Zn^{+2} with inserted silicate nanoparticles. Also, the annealing process involves the release of solvent, which might assist chain packing into secondary crystallites. It appears that silicate particle insertion does not significantly interfere with secondary or primary crystallization in the sense that both crystalline entities persist. This conclusion is in harmony with the noninterpenetrating nature of the silicate phase as given evidence by the well-defined spherical nature of the nanoparticles.[31]

TGA

The TGA thermograms of the unfilled and hybrid samples seen in Figure 14 show essentially no change in the temperature of the onset of degradation. The mass of the hybrids remains constant at temperatures > 475°C, which is typical of a silicate component at these temperatures that are low and nondegradative relative to inorganic oxide glasses. While the degradation onset temperature is rather invariant, higher temperatures are required for the organic phase of the hybrids to totally degrade, which might imply interactions between the organic and inorganic components near the phase boundaries. An alternative view is that this "extra" weight loss is due to water that is released because of temperature-driven condensation reactions between uncondensed SiOH groups. In any case, these results imply a considerable degree of organic/inorganic phase separation in the sense of noninterpenetration. No mass whatsoever is retained above 475°C

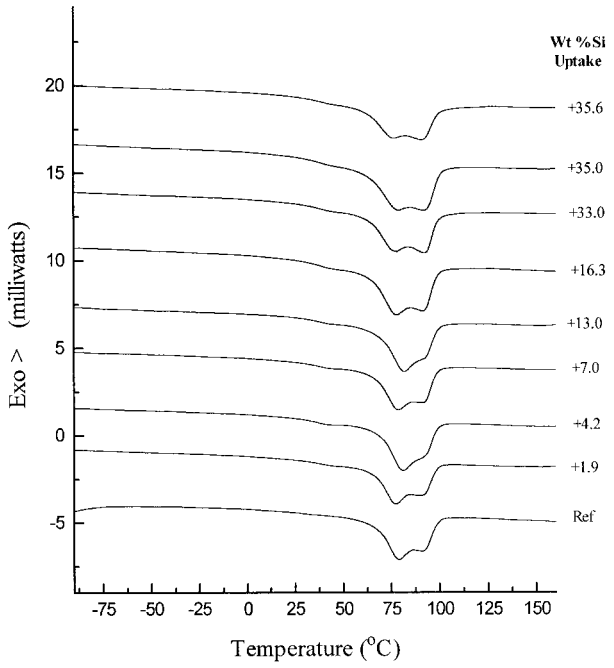

Figure 13 First scan DSC thermograms of Surlyn®–Zn^{2+}/silicate hybrids with the indicated inorganic percentage uptakes.

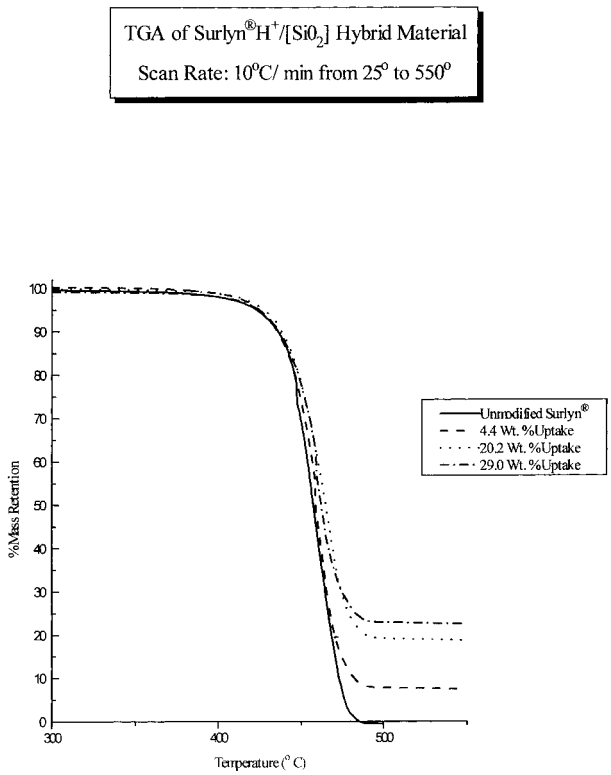

Figure 14 TGA thermograms (10°C/min) of Surlyn®–H/silicate hybrids with the indicated compositions plus an unfilled Surlyn®–H control sample.

for the unfilled copolymer, and the residual mass fraction for the hybrid specimens above this temperature is commensurate with the initial silicate filler content.

CONCLUSIONS

Selected exploratory experiments demonstrated that Surlyn®/silicate hybrids are achievable via polymer *in situ* sol–gel reactions for TEOS. FTIR spectra provided evidence of and limited information in regard to silicate structures that were incorporated in both the acid and Zn^{+2} forms of Surlyn®. All of the fingerprint bands of a silicate phase were present and, given the detection of a considerable population of SiOH groups, incomplete molecular connection existed within this nanophase. In future studies this structural aspect will be manipulated via the pH, water concentration, and drying conditions. The —COOH dimerization in Surlyn®-H was rather complete at room temperature and the *in situ* sol–gel process that led to silicate incorporation did not change this condition. The absence of frequency shifting of Surlyn®-H associated bands with the incorporation of the silicate component implied that strong interactions *on the molecular level* between the organic and inorganic phases were not present or weak. However, the phases must be mechanically coupled on a larger dimensional scale as indicated by our experiments that showed a monotonic increase in mechanical tensile modulus with increasing silicate content.

The ^{29}Si solid-state NMR analyses indicated mainly Q_3 and Q_4 coordination states, regardless of silicate content, which was in general agreement with the interpretation of the FTIR results that showed incomplete condensation. From this considerable degree of molecular disconnection, we inferred that an ill-defined porosity was present. The ESEM/EDAX evidence reinforced the conclusion arrived at by spectroscopic means: it is possible to incorporate a significant silicate component through the depth of the films.

First-scan DSC thermograms for Surlyn®-Zn^{+2}/silicate hybrids revealed two distinct melting endotherms similar to those seen for unmodified Surlyn®. It appeared that silicate particle insertion in this way does not significantly interfere with crystallinity, which was in harmony with the well-defined spherical geometry observed for the nanoparticles. The TGA of unfilled Surlyn® and hybrid samples showed essentially no change in the temperature of the onset of thermal degradation, which implied that a considerable degree of organic/inorganic phase separation existed.

Future experiments will include similar utilization of *in situ* sol–gel processes to generate titania and mixed silica-titania nanophases in Surlyn® matrices.

The authors acknowledge the support of the Mississippi NSF-EPSCoR program and partial support by E. I. DuPont de Nemours & Co. We also acknowledge the assistance given in the acquisition and interpretation of the ^{29}Si solid-state NMR spectra by W. L. Jarrett, Department of Polymer Science, University of Southern Mississippi.

REFERENCES

1. Wilson, F. W.; Longworth, R.; Vaughan, D. J Am Chem Soc Polym Prepr 1968, 9, 505.
2. Longworth, R.; Vaughan, D. J. Nature 1968, 218, 85.
3. (a) Longworth, R.; Nagel, H. In Ionomers: Synthesis, Structure, Properties and Applications; Tant, M. R., Mauritz, K. A., Wilkes, G. L., Eds.; Blackie

Academic & Professional: London, 1997; Chap. 9; (b) Longworth, R. In The Wiley Encyclopedia of Packaging Technology; Wiley: New York, 1986; p 421.
4. (a) Rees, R. W. In Engineered Materials Handbook, Engineering Plastics; ASM International, Materials Park, OH, 1987; Vol. 2, p 120; (b) Encyclopedia of Polymer Science and Engineering; ASM International Handbook Committee; Wiley: New York, 1987; Vol. 8, p 395.
5. Modern Plastics Encyclopedia, McGraw–Hill: New York, 1981–1982; p 27.
6. Tadano, K.; Hirasawa, E.; Yamamoto, H.; Yano, S. Macromolecules 1989, 22, 226.
7. Tachino, H.; Hara, H.; Hirasawa, E.; Kutzumizu, S.; Tadano, K.; Yano, S. Macromolecules 1993, 26, 752.
8. Kutsumizu, S.; Nagao, N.; Tadano, K.; Tachino, H.; Hirasawa, E.; Yano, S. Macromolecules 1992, 25, 6829.
9. Kutsumizu, S.; Hara, H.; Tachino, H.; Shimabayashi, K.; Yano, S. Macromolecules 1999, 32, 6340.
10. Eisenberg, A.; Hird, B.; Moore, R. B. Macromolecules 1990, 23, 4098.
11. Marx, C. L.; Cooper, S. L. J Macromol Sci Phys Ed 1974, B9, 19.
12. Goddard, R. J.; Grady, B. P.; Cooper, S. L. Macromolecules 1994, 27, 1710.
13. Loo, Y.-L.; Register, R. A. Am Chem Soc Div Polym Sci Eng Prepr 1999, 81, 294.
14. Qiu, G.; Tang, Z.-L.; Huang, N.-X.; Gerking, L. J Appl Polym Sci 1998, 69, 729.
15. Otocka, E. P.; Kwei, T. K.; Salovey, R. Makromol Chem 1969, 129, 144.
16. Mauritz, K. A.; Jones, C. K. J Appl Polym Sci 1990, 40, 1401.
17. Mauritz, K. A.; Ju, R. Chem Mater 1994, 6, 2269.
18. Juangvanich, N.; Mauritz, K. A. J Appl Polym Sci 1998, 67, 1799.
19. Mauritz, K. A.; Warren, R. M. Macromolecules 1989, 22, 4483.
20. Mauritz, K. A.; Stefanithis, I. D.; Davis, S. V.; Scheetz, R. W.; Pope, R. K.; Wilkes, G. L.; Huang, H.-H. J Appl Polym Sci 1995, 55, 181.
21. Gummaraju, R. V.; Moore, R. B.; Mauritz, K. A. J Polym Sci B Polym Phys Ed 1996, 34, 2383.
22. Shao, P. L.; Mauritz, K. A.; Moore, R. B. Chem Mater 1995, 7, 192.
23. Shao, P. L.; Mauritz, K. A.; Moore, R. B. J Polym Sci B Polym Phys 1996, 34, 873.
24. Apichatachutapan, W.; Moore, R. B.; Mauritz, K. A. J Appl Polym Sci 1996, 62, 417.
25. Deng, Q.; Moore, R. B.; Mauritz, K. A. Chem Mater 1995, 7, 2259.
26. Deng, Q.; Jarrett, W.; Moore, R. B.; Mauritz, K. A. J Sol–Gel Sci Technol 1996, 7, 177.
27. Deng, Q.; Mauritz, K. A.; Moore, R. B. In Hybrid Organic–Inorganic Composites, ACS Symposium Series 585; Mark, J. E., Bianconi, P. A., Lee, C. Y.-C., Eds.; American Chemical Society: Washington, DC, 1995; Chap. 7.
28. Greso, A. J.; Moore, R. B.; Cable, K. M.; Jarrett, W. L.; Mauritz, K. A. Polymer 1997, 38, 1345.
29. Robertson, M. A. F.; Mauritz, K. A. J Polym Sci B Polym Phys 1998, 36, 595.
30. (a) Payne, J. T.; Reuschle, D. A.; Brister, L. B.; Curry, C. L.; Shoemake, K. A.; Storey, R. F.; Mauritz, K. A. Am Chem Soc Div Polym Chem Prepr 1997, 38, 249; (b) Reuschle, D. A.; Mountz, D. A.; Mauritz, K. A.; Brister, L. B.; Storey, R. F.; Beck Tan, N. Am Chem Soc Div Polym Chem Prepr 1999, 40, 713; (c) Mountz, D. A.; Reuschle, D. A.; Storey, R. F.; Mauritz, K. A. Am Chem Soc Div Polym Chem Prepr 1999, 40, 892.
31. Start, P.; Mauritz, K. A. Am Chem Soc Div Polym Chem Prepr 1998, 39, 375.
32. Siuzdak, D. A.; Mauritz, K. A. J Polym Sci B Polym Phys 1999, 37, 143.
33. Cory, D. G.; Ritchey, W. M. J Magn Reson 1988, 80, 128.
34. Earnest, T. R.; MacKnight, W. J. Macromolecules 1980, 13, 844.
35. Brozoski, B. A.; Coleman, M. M.; Painter, P. C. Macromolecules 1984, 17, 230.
36. Painter, P. C.; Brozoski, B. A.; Coleman, M. M. J Polym Sci B Polym Phys 1982, 20, 1074.
37. Painter, P. C.; Coleman, M. M. Fundamentals of Polymer Science; Technomic: Lancaster, PA, 1994; p 155.
38. Painter, P. C.; Watzelk, M.; Koenig, J. L. Polymer 1977, 18, 1169.
39. Van Alsten, J. G. Macromolecules 1996, 29, 2163.
40. Conley, R. T. Infrared Spectroscopy, 2nd ed.; Allyn & Bacon: Boston, 1975; p 176.
41. Smith, A. L. Spectrochim Acta 1960, 16, 87.
42. Anderson, D. R. In Analysis of Silicones; Smith, A. L., Ed.; Wiley–Interscience: New York, 1974; Chap. 10.
43. Conley, R. T. Infrared Spectroscopy, 2nd ed.; Allyn & Bacon: Boston, 1975; p 161.
44. Coleman, M. M.; Graf, J. F.; Painter, P. C. Specific Interactions and the Miscibility of Polymer Blends; Technomic: Lancaster, PA, 1991; p 239.
45. Conley, R. T. Infrared Spectroscopy, 2nd ed.; Allyn & Bacon: Boston, 1975; p 99.